THE JOURNAL OF PHYSICAL CHEMISTRY Letters

Letter

Cite This: J. Phys. Chem. Lett. 2019, 10, 4339−4344

pubs.acs.org/JPCL

Resonant Two-Photon Photoelectron Imaging and Intersystem Crossing from Excited Dipole-Bound States of Cold Anions

Guo-Zhu Zhu, Ling Fung Cheung, Yuan Liu, Chen-Hui Qian, and Lai-Sheng Wang*

Department of Chemistry, Brown University, Providence, Rhode Island 02912, United States

Supporting Information

ABSTRACT: We report the observation of a dipole-bound state (DBS) 659 cm^{-1} below the electron detachment threshold of cryogenically cooled deprotonated 4,4′-biphenol anion (bPh^-) and 19 of its lowest vibrational levels. Resonant two-photon photoelectron imaging (R2P-PEI) via the vibrational levels of the DBS displays a sharp peak with a constant binding energy. This observation indicates vertical detachment from the vibrational levels of the DBS to the corresponding neutral levels with the conservation of the vibrational energy, suggesting that the highly diffuse electron in the DBS has little effect on the neutral core. The R2P-PEI spectra also exhibit two features at lower binding energies, which come from intersystem crossings from the DBS to two lower-lying valence-bound triplet excited states of bPh^-. The current study discloses the first R2P-PEI spectra from vibrational excited states of a DBS and direct spectroscopic evidence of transitions from a DBS to valence-bound states of anions.

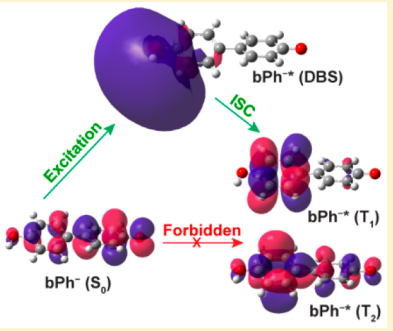

Anions with a polar neutral core (μ > ~2.5 D) can have an excited dipole-bound state (DBS) just below the electron detachment threshold,[1,2] analogous to Rydberg states for neutral molecules. The electron in a DBS is weakly bound in a diffuse orbital by the long-range charge−dipole interaction between the electron and the dipolar neutral core. Since first proposed by Fermi and Teller in 1947,[3] DBS has attracted persistent attention because of its fundamental importance in physics and chemistry.[4−6] It has been considered as the "doorway" to form conventional valence-bound anions,[7−9] and it plays significant roles in understanding reductive DNA damage by low-energy electron attachment[10] and anion formation in the interstellar medium.[11,12]

The transition from a DBS to a valence-bound state (VBS) was first considered both theoretically and experimentally for $CH_3NO_2^-$,[7,8] in which the ground-state dipole-bound anion (DBA) was formed via Rydberg electron transfer and probed by electric-field-induced detachment, while the VBS was investigated by photoelectron spectroscopy (PES).[8] Photoelectron (PE) spectra of ground-state DBAs usually display a single sharp peak with very low electron binding energies, because there is little geometry change between the DBS and the neutral core, while those of valence-bound anions give broad PES features due to Franck−Condon activities proportional to the geometry changes between the anionic and neutral ground states.[13] The dynamics involving transitions from DBS to VBS was first investigated for iodide−water cluster anions $[I^-(H_2O)_n]$ using time-resolved PES.[14] The electron initially localized on the I^- anion is excited to the DBS of the water network, which is isomerized to a lower-energy conformer of the water cluster along with an electronic transition to a lower-energy VBS. Several time-resolved PES experiments have been done recently for anion clusters of I^-, such as $I^-\cdot CH_3NO_2$ (ref 15) and iodide−nucleobase complexes,[10] revealing a time scale of several picoseconds for the DBS-to-VBS transition. Similar time-resolved PES has been used to probe the dynamics of transition from a nonvalence correlation-bound state (CBS) to VBS in $I^-{-}C_6F_6$ complexes, uncovering even faster time scales from a few tens of femtoseconds to a few hundred femtoseconds.[16]

The previous experimental studies concerning the dynamics of DBS or CBS involve electronic excitations from an anionic chromophore (e.g., I^-) in an anionic complex to a diffuse state on the solvent part of the complex and its relaxation to the ground VBS.[10,14,15] Here we report spectroscopic observations of electronic transitions from an excited DBS to VBS in an isolated molecular anion [deprotonated 4,4′-biphenol anion (bPh^-), inset of Figure 1a], using high-resolution photoelectron imaging (PEI) and photodetachment spectroscopy.[17] The experiment was carried out using an electrospray-PES apparatus, which consists of an electrospray ionization source, a cryogenically cooled Paul trap,[18] and a high-resolution PEI system[19] (see more details in the Supporting Information). Nonresonant PEI was used to yield the electron affinity (EA) of the bPh radical and the Franck−Condon activity between anion and neutral ground states. Photodetachment spectroscopy revealed a DBS of bPh^- 659 cm^{-1} below its detachment threshold along with 19 vibrational levels of the excited DBS across the detachment threshold. Resonant two-photon photoelectron imaging (R2P-PEI) was obtained for the below-threshold DBS vibrational levels, showing a sharp peak with a constant binding energy due to vertical detachment from the DBS vibrational levels to the respective neutral levels.

Received: June 16, 2019
Accepted: July 17, 2019
Published: July 17, 2019

DOI: 10.1021/acs.jpclett.9b01743
J. Phys. Chem. Lett. 2019, 10, 4339−4344

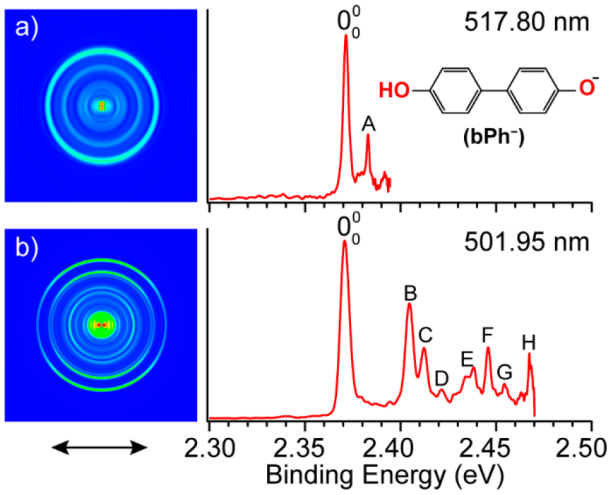

Figure 1. Photoelectron images and spectra of bPh^- at (a) 517.80 nm and (b) 501.95 nm. The double arrow below the images indicates the directions of the laser polarization.

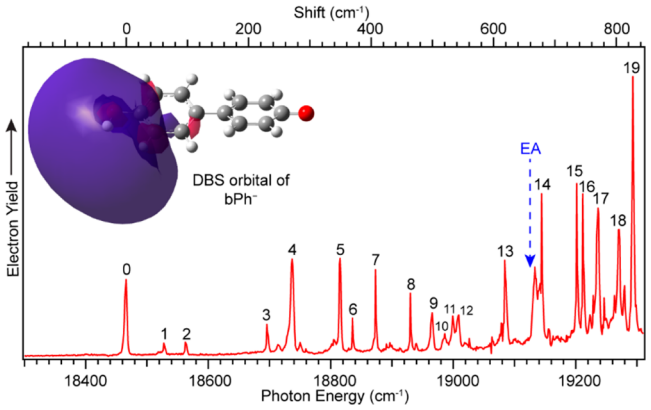

Figure 2. Photodetachment spectrum of bPh^-. The observed peaks indicate the vibrational levels of an electronically excited DBS just below the detachment threshold of bPh^- (the dashed arrow). Peak 0 is the ground vibrational level of the DBS, 659 cm^{-1} below the threshold. The inset shows the diffuse *s*-type dipole-bound orbital calculated for bPh^-.

Two additional peaks were also observed in the R2P-PEI spectra, suggesting intersystem crossings from the DBS to two low-lying excited triplet states of bPh^-. In addition, single-photon resonant PES was conducted for the above-threshold vibrational resonances, revealing vibrational-specfic autodetachment.

Figure 1 shows the nonresonant PE images and spectra of bPh^- at two photon energies. The lowest binding energy peak (0_0^0) represents the detachment transition from the ground state of bPh^- to that of neutral bPh, yielding an accurate electron affinity (EA) for the bPh radical (2.3712 eV or 19125 cm^{-1}). The higher binding energy peaks, labeled from A to H, indicate vibrational excitations of neutral bPh governed by the Franck–Condon principle. The most Franck–Condon-active mode (ν_6, represented by the intense peak B) involves C–C and C–O stretches within each phenol moiety (Figure S1). The major geometry changes upon electron detachment consist of slight shortening of the C–C bonds and the C–O bonds, consistent with the highest occupied molecular orbital (HOMO) of bPh^- (Figure S2c), which describes antibonding $\pi-\pi$ interactions within each phenyl ring and between the phenyl rings and the terminal O atoms. The binding energies of all the observed vibrational peaks and their assignments are given in Table S1. In addition to ν_6, three more fundamental vibrational modes (ν_3, ν_{11}, and ν_{19}, Figure S1) are also observed with weak Franck–Condon activities, represented by peaks A, D, and G, respectively. The remaining peaks consist of overtones of ν_6 or combinational vibrational levels (Table S1).

The deprotonated bPh neutral radical is calculated to have a dipole moment of 6.35 D, large enough to support an excited DBS for the bPh^- anion. Figure 2 shows the photodetachment spectrum of bPh^-, obtained by measuring the total electron yield as a function of photon energy across the detachment threshold. A dipole-bound excited state was indeed observed, 695 cm^{-1} below the electron detachment threshold (indicated by the dashed arrow). A total of 20 DBS vibrational resonances, labeled as 0–19, are observed in the scanned photon energy range. As discussed previously,[20−22] the below-threshold resonances, labeled as 0–13, are due to resonant two-photon processes. Peak 0, below the detachment threshold by 659 cm^{-1}, is the ground vibrational level of the DBS. The 659 cm^{-1} binding energy of the DBS is quite high, consistent with the large dipole moment of bPh. Above threshold, the continuously increasing baseline represents the cross section of nonresonant one-photon detachment processes, while peaks 14–19 (aka vibrational Feshbach resonances) indicate one-photon excitations to the DBS vibrational levels followed by vibrationally induced autodetachment. The wavelengths and photon energies of the DBS vibrational resonances are given in Table S2.

By tuning the detachment laser wavelengths to the vibrational resonances observed in Figure 2, we obtained R2P-PE spectra for the below-threshold resonances (peaks 0–13) and resonantly enhanced PE spectra for the vibrational Feshbach resonances (peaks 14–19), as shown in Figure 3. The resonant PE spectra corresponding to the Feshbach resonances are mainly from vibrational autodetachment after one-photon excitation following the $\Delta v = -1$ propensity rule,[23,24] resulting in photoelectrons with high binding energies (Figure 3b; also see Figure S3 for high-resolution PE images and spectra). The R2P-PE spectra corresponding to the below-threshold resonances primarily consist of low binding energy (high kinetic energy) photoelectrons due to two-photon detachment. The binding energies are obtained by subtracting the electron kinetic energies from the photon energy used even for the two-photon spectra.

Previous experiments[20−22] have shown that the electron weakly bound in the DBS exerts little effect on the neutral core; that is, the structures of the dipole-bound anion and the neutral radical are similar. Here, this structural similarity is demonstrated by the matching of major DBS vibrational resonances of bPh^- with the vibrational peaks of the bPh neutral resolved in the PE spectrum, as compared in Figure S4. As shown previously,[20−22] the vibrational frequencies of the DBS and the corresponding neutral core are the same within our experimental accuracy (±5 cm^{-1}). Hence, the computed vibrational frequencies for the neutral bPh (Table S3) can be used to guide the assignments of the DBS resonances of bPh^-. The assignments of the above-threshold DBS vibrational levels are also confirmed by resonant PES (vide infra) based on the vibrational peaks enhanced in the resonant PE spectra (Figures 3b and S3) and the propensity rule of $\Delta v = -1$ for vibrational autodetachment from the DBS resonances.[20−24] It should be noted that a prime is used to designate the vibrational levels of

DOI: 10.1021/acs.jpclett.9b01743
J. Phys. Chem. Lett. 2019, 10, 4339–4344

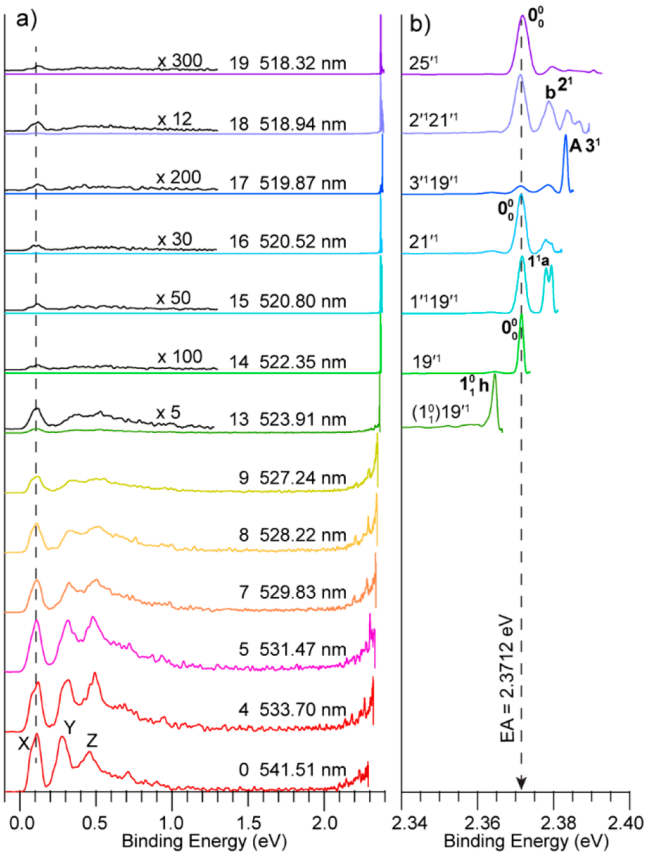

Figure 3. R2P-PE spectra of bPh^- at wavelengths corresponding to the DBS vibrational levels in Figure 2. (a) Full spectra showing both the low and high binding energy features. The dashed line indicates the constant binding energy of peak X at all detachment wavelengths. (b) Expanded spectra in the binding energy range of 2.34−2.40 eV, showing the one-photon spectra for the above-threshold resonances. The dashed arrow indicates the detachment threshold. Peaks labeled in boldface type indicate the enhanced vibrational peaks in comparison to the nonresonant spectra in Figure 1. The vibrational levels for the above-threshold DBS resonances are also given.

the DBS to be distinguished from the same vibrational levels of the neutral.

In comparison to the nonresonant spectra shown in Figure 1, the high binding energy part of the spectra (Figure 3b) at laser wavelengths corresponding to the Feshbach resonances 14−19 in Figure 2 are highly non-Franck−Condon, because of the $\Delta v = -1$ propensity rule for vibrationally induced autodetachment,[20−24] resulting in enhanced neutral vibrational peaks (labeled in boldface type in Figure 3b; also see Figure S3). The 0_0^0 peak is enhanced in the spectra at 522.35 nm (resonance 14), 520.52 nm (resonance 16), and 518.32 nm (resonance 19), because of excitations to the $19'^1$, $21'^1$, and $25'^1$ vibrational levels of the DBS, respectively. The other three above-threshold resonant PE spectra are due to excitations to combinational vibrational modes of the DBS. The resonantly enhanced peaks **a** (1^1), **b** (2^1), and **A** (3^1) represent fundamental excitations of the first three lowest-frequency vibrational modes of neutral bPh (Table S3). Specifically, the lowest-frequency torsional modes (ν_1 and ν_2) are not observed in the nonresonant PE spectra (Figure 1), which demonstrates the power of resonant PES to obtain greater vibrational information for neutral radical species.[20−22] The resonant PE spectrum for the below-threshold resonance 13 at 523.91 nm shows that peak **h** is enhanced, which is red-shifted by −55 cm^{-1} relative to peak 0_0^0, i.e. because of a vibrational hot band of the ν_1 mode (1_1) in combination with the excitation of one quantum of the ν_{19} mode ($1_1^0 19'^1$). The population of the lowest-frequency ν_1 mode in the anion is consistent with the vibrational temperature of 30−35 K for anions in our cryogenically cooled Paul trap.[25,26] In addition to the enhanced PES peaks, very weak signals at low BE are also observed in the above-threshold spectra (Figure 3a; also see Figure S5 for the R2P-PE images and the expanded spectra), which must be due to two-photon processes, as described below. The autodetachment processes involving the enhancement of peak 0_0^0 are schematically displayed in Figure 4a, while a complete schematic energy level diagram is given in Figure S7.

For the below-threshold DBS resonances, two photons are required for electron detachment: the first photon excites the anion from the ground state of bPh^- to specific vibrational levels of the DBS followed by the second photon to detach the electron, resulting in electrons with very high kinetic energies. A single vibrational peak is expected for the resonant two-

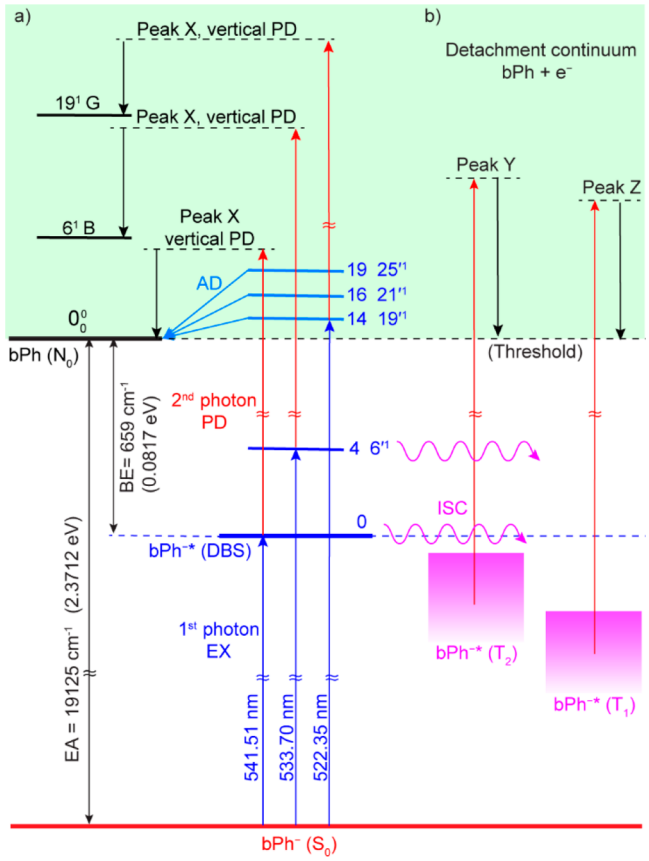

Figure 4. Schematic energy level diagram showing different detachment processes of bPh^-. (a) Assignments of several vibrational levels of bPh and the DBS resonances observed for bPh^- in Figure 2. The autodetachment (AD) processes from the above-threshold DBS vibrational levels of bPh^-, reached via single-photon excitations (EX) from the ground state of bPh^-, are indicated. R2P processes via the DBS ground and excited vibrational levels to the corresponding neutral vibrational levels are indicated for peak X. (b) Intersystem crossing (ISC) from the DBS to the two triplet excited states (T_1 and T_2) of bPh^- is indicated, as is the photodetachment by the second photon giving rise to peaks Y and Z. The shaded area above the threshold indicates the detachment continuum.

DOI: 10.1021/acs.jpclett.9b01743
J. Phys. Chem. Lett. 2019, 10, 4339−4344

photon spectra because there is little geometry change between the DBS and the neutral state, as has been observed previously for the resonant two-photon detachment via the ground vibrational levels of many DBS's.[20−22] Surprisingly, three peaks (X, Y, and Z) are observed for all the below-threshold resonances, and to a lesser extent even for the above-threshold spectra, as shown in Figure 3a.

The binding energies of the three features in the two-photon spectra at 541.51 nm, corresponding to the ground vibrational level of the DBS, are 0.103 (±0.040), 0.283 (±0.040), and 0.458 (±0.042) eV, for X, Y, and Z, respectively (Figure 3a). The binding energy of peak X measured in this low-resolution spectrum is consistent with the binding energy of the DBS measured more accurately as 659 cm^{-1} (0.0817 eV) from the photodetachment spectrum (Figure 2). This means that peak X corresponds to R2P detachment via the ground vibrational level of the DBS. This is confirmed by the p-wave angular distribution in the R2P-PE image (Figure S6), because of the *s*-type DBS orbital (see inset of Figure 2). More specifically, the anisotropy parameter β is found to be 1.1, relative to 2 for a pure p-wave.

More surprisingly, when we tune the laser to reach the excited vibrational levels of the DBS, e.g. to resonances 4, 5, 7, 8, 9, and 13, a similar peak X is observed with the same binding energy (Figure 3a). Even for all the above-threshold R2P-PE spectra, the peak X is observed, albeit at much weaker intensities. There are two possible explanations. One suggests that the vibrationally excited states of the DBS has radiatively relaxed to the ground vibrational level of the DBS within the 5 ns laser pulse used, followed by absorption of a second photon detaching the DBS electron from the vibrational ground state regardless of the vibrational levels reached by the first photon. The weak peak X at the above-threshold R2P-PE spectra further indicates that the time scale of the vibrational relaxation would compete with that of the vibrational-induced autodetachment, which was estimated to be on the order of picoseconds.[25,27] However, radiative vibrational relaxation times for isolated molecules are usually on the order of milliseconds or even longer.[28−30] Hence, the required fast vibrational radiative relaxation seems unlikely.

A more likely explanation is the vertical detachment from the excited vibrational levels of the DBS to those of the neutral with the conservation of the vibrational energy.[31] As schematically shown in Figure 4a, after the first photoexcitation from the anion ground state to the DBS vibrational levels, the electron is detached by the second photon from the DBS vibrational levels to the corresponding neutral vibrational levels (specifically, $6'^1$ to 6^1 and $19'^1$ to 19^1). The R2P detachment processes yield a constant binding energy for peak X, regardless of the wavelengths used. It can also be understood that the second photon detaches the DBS electron without perturbing the vibrationally excited neutral core (strictly vertical transition), further indicating the weakly bound nature of the DBS electron even with a relative high binding energy of 659 cm^{-1}. It is interesting to note that the R2P-PES via the excited vibrational levels of the DBS is totally different from that via an excited valence excited state, such as in AuS^-, where vibrational state-selective R2P-PE spectra were obtained with very different Franck−Condon distributions depending on the vibrational levels reached in the intermediate state.[32]

The PE images of peaks Y and Z are relatively isotropic with β values of ∼0.1 (Figure S6), different from that of peak X, suggesting that they have different electronic origins. The observation of these higher binding energy features implies the existence of lower-lying valence excited states, which are populated via the DBS through intramolecular vibrational redistribution or intersystem crossing. To search for low-lying electronic excited states of bPh^-, we carried out theoretical calculations using time-dependent density functional theory at the geometry of the anion ground state optimized under two different methods, B3LYP/6-311++G(d,p) and TPSSH/6-311++G(d,p).[33,34] We indeed found one singlet (S_1) and two triplet (T_1, T_2) excited states near the detachment threshold with vertical excitation energies given in Table S4. The calculated potential energy curves along the dihedral angle (C1−C2−C3−C4) of the two phenyl rings are shown in Figure S2a for the anion ground state (S_0), the singlet exited state (S_1), the two triplet excited states (T_1 and T_2), and the neutral ground state (N_0). There is little change in the dihedral angle between the anion ground state and that of the neutral, as seen by the S_0 and N_0 curves. The DBS curve should be parallel and slightly below the N_0 curve by 659 cm^{-1} (0.0817 eV). At the equilibrium geometry of the N_0 curve, the S_1 state is higher in energy (above the detachment threshold) and also has little Franck−Condon overlap with the DBS, thus excluding the possibility of the S_1 state for the observed peaks Y and Z. On the other hand, the T_1 and T_2 potential energy curves both have good overlaps with the double wells of the neutral N_0 curve and consequently should have good overlap with the DBS. Hence, the T_1 and T_2 states are likely populated via intersystem crossings from the DBS and give rise to peaks Y and Z upon detachment by the second photon, as schematically shown in Figure 4b.

The T_1 and T_2 states correspond to excitations of an electron from the HOMO to the lowest unoccupied molecular orbital (LUMO) and LUMO+1 (Figure S2b) of bPh^-, respectively, which are both p-type π^* orbitals (Figure S2c). Detachment from the p-type orbitals is expected to give rise to s+d waves for the outgoing photoelectrons, consistent with the angular distributions of peaks Y and Z (Figure S6). The calculated excitation energies are in reasonable agreement with the experimental values (Table S4). The transitions from the DBS to the T_1 and T_2 states, via the intersystem crossing (ISC) (Figure 4b), is spin-forbidden.[35,36] The high probability for the intersystem crossing is another illustration of the weak spin coupling between the dipole-bound electron in the DBS and the neutral core.[37] Direct excitations from the bPh^- anion ground state to the T_1 and T_2 excited states are spin-forbidden, which is why they are not observed in the photodetachment spectrum in Figure 2. Peaks Y and Z become broadened for the vibrationally excited levels of the DBS (Figure 3a), which suggests that, in addition to vertical R2P detachment, direct ISC from these levels to highly vibrationally excited T_1 and T_2 states is also possible, as schematically shown for resonance 4 in Figure 4. Intramolecular vibrational energy redistributions and relaxations can occur in the T_1 and T_2 states before being detached by the second photon, resulting in the broader Y and Z peaks.[38]

In conclusion, we have observed an excited DBS for the deprotonated 4,4′-biphenol anion (bPh^-) and observed 20 vibrational levels. A total of 13 fundamental vibrational modes are observed for the bPh neutral radical from the photodetachment spectroscopy and resonant photoelectron spectroscopy. Resonant two-photon detachment spectra via the vibrational resonances revealed vertical photodetachment from the excited vibrational levels of the DBS to the corresponding

DOI: 10.1021/acs.jpclett.9b01743
J. Phys. Chem. Lett. 2019, 10, 4339−4344

neutral vibrational levels, further demonstrating that the DBS electron exerts little effect on the excited neutral core. Spectroscopic and theoretical evidence was provided for intersystem crossings from the DBS to two low-lying valence-bound triplet excited states of bPh^-. The current work suggests that a pump−probe experiment is feasible to investigate both the dynamics of the intersystem from dipole-bound excited states to valence-bound excited states, as well as dynamics of vibrationally induced autodetachment.

■ ASSOCIATED CONTENT

Supporting Information

The Supporting Information is available free of charge on the ACS Publications website at DOI: 10.1021/acs.jpclett.9b01743.

Experimental and theoretical methods; calculated vibrational modes and frequencies of bPh neutral radical; calculated excitation energies, potential energy surfaces, and molecular orbitals of electronic states of bPh^-; comparison of photodetachment spectrum and nonresonant photoelectron spectrum; high-resolution PE images and spectra of above-threshold DBS resonances; R2P-PE images and expanded spectra; a complete energy level diagram; and a summary of observed vibrational peaks and DBS resonances (PDF)

■ AUTHOR INFORMATION

Corresponding Author

*E-mail: Lai-Sheng_Wang@brown.edu.

ORCID

Yuan Liu: 0000-0003-1468-942X

Lai-Sheng Wang: 0000-0003-1816-5738

Notes

The authors declare no competing financial interest.

■ ACKNOWLEDGMENTS

This work was supported by the U.S. Department of Energy, Office of Basic Energy Sciences, Chemical Sciences, Geosciences, and Biosciences Division under Grant DE-SC0018679.

■ REFERENCES

(1) Jackson, R. L.; Hiberty, P. C.; Brauman, J. I. Threshold Resonances in the Electron Photodetachment Spectrum of Acetaldehyde Enolate Anion. Evidence for a Low-Lying, Dipole-Supported State. *J. Chem. Phys.* **1981**, *74*, 3705−3712.

(2) Lykke, K. R.; Mead, R. D.; Lineberger, W. C. Observation of Dipole-Bound States of Negative Ions. *Phys. Rev. Lett.* **1984**, *52*, 2221−62224.

(3) Fermi, E.; Teller, E. The Capture of Negative Mesotrons in Matter. *Phys. Rev.* **1947**, *72*, 399−408.

(4) Desfrancois, C.; Abdoul-Carime, H.; Schermann, J. P. Ground-State Dipole-Bound Anions. *Int. J. Mod. Phys. B* **1996**, *10*, 1339−1395.

(5) Jordan, K. D.; Wang, F. Theory of Dipole-Bound Anions. *Annu. Rev. Phys. Chem.* **2003**, *54*, 367−396.

(6) Simons, J. Molecular Anions. *J. Phys. Chem. A* **2008**, *112*, 6401−66511.

(7) Gutsev, G. L.; Bartlett, R. J. A Theoretical Study of the Valence- and Dipole-Bound States of the Nitromethane Anion. *J. Chem. Phys.* **1996**, *105*, 8785−8792.

(8) Compton, R. N.; Carman, J. H. S.; Desfrancois, C.; Abdoul-Carime, H.; Schermann, J. P.; Hendricks, J. H.; Lyapustina, S. A.; Bowen, K. H. On the Binding of Electrons to Nitromethane: Dipole and Valence Bound Anions. *J. Chem. Phys.* **1996**, *105*, 3472−3478.

(9) Sommerfeld, T. Coupling between Dipole-Bound and Valence States: The Nitromethane Anion. *Phys. Chem. Chem. Phys.* **2002**, *4*, 2511−2516.

(10) Kunin, A.; Neumark, D. M. Time-Resolved Radiation Chemistry: Femtosecond Photoelectron Spectroscopy of Electron Attachment and Photodissociation Dynamics in Iodide−Nucleobase Clusters. *Phys. Chem. Chem. Phys.* **2019**, *21*, 7239−7255.

(11) Güthe, F.; Tulej, M.; Pachkov, M. V.; Maier, J. P. Photodetachment Spectrum of l-$C_3H_2^-$: The Role of Dipole Bound States for Electron Attachment in Interstellar Clouds. *Astrophys. J.* **2001**, *555*, 466−471.

(12) Fortenberry, R. C. Interstellar Anions: The Role of Quantum Chemistry. *J. Phys. Chem. A* **2015**, *119*, 9941−9953.

(13) Hendricks, J. H.; Lyapustina, S. A.; de Clercq, H. L.; Bowen, K. H. The Dipole Bound-to-Covalent Anion Transformation in Uracil. *J. Chem. Phys.* **1998**, *108*, 8−11.

(14) Lehr, L.; Zanni, M. T.; Frischkorn, C.; Weinkauf, R.; Neumark, D. M. Electron Solvation in Finite Systems: Femtosecond Dynamics of Iodide·(Water)$_n$ Anion Clusters. *Science* **1999**, *284*, 635−638.

(15) Yandell, M. A.; King, S. B.; Neumark, D. M. Decay Dynamics of Nascent Acetonitrile and Nitromethane Dipole-Bound Anions Produced by Intracluster Charge-Transfer. *J. Chem. Phys.* **2014**, *140*, 184317.

(16) Rogers, J. P.; Anstöter, C. S.; Verlet, J. R. R. Ultrafast Dynamics of Low-Energy Electron Attachment via a Non-Valence Correlation-Bound State. *Nat. Chem.* **2018**, *10*, 341−346.

(17) Wang, L. S. Perspective: Electrospray Photoelectron Spectroscopy: From Multiply-Charged Anions to Ultracold Anions. *J. Chem. Phys.* **2015**, *143*, 040901.

(18) Wang, X. B.; Wang, L. S. Development of a Low-Temperature Photoelectron Spectroscopy Instrument Using an Electrospray Ion Source and a Cryogenically Controlled Ion Trap. *Rev. Sci. Instrum.* **2008**, *79*, 073108.

(19) León, I.; Yang, Z.; Liu, H. T.; Wang, L. S. The Design and Construction of a High-Resolution Velocity-Map Imaging Apparatus for Photoelectron Spectroscopy Studies of Size-Selected Clusters. *Rev. Sci. Instrum.* **2014**, *85*, 083106.

(20) Liu, H. T.; Ning, C. G.; Huang, D. L.; Dau, P. D.; Wang, L. S. Observation of Mode-Specific Vibrational Autodetachment from Dipole-Bound States of Cold Anions. *Angew. Chem., Int. Ed.* **2013**, *52*, 8976−8979.

(21) Huang, D. L.; Liu, H. T.; Ning, C. G.; Zhu, G. Z.; Wang, L. S. Probing the Vibrational Spectroscopy of the Deprotonated Thymine Radical by Photodetachment and State-Selective Autodetachment Photoelectron Spectroscopy via Dipole-Bound States. *Chem. Sci.* **2015**, *6*, 3129−3138.

(22) Zhu, G. Z.; Qian, C. H.; Wang, L. S. Dipole-Bound Excited States and Resonant Photoelectron Imaging of Phenoxide and Thiophenoxide Anions. *J. Chem. Phys.* **2018**, *149*, 164301.

(23) Berry, R. S. Ionization of Molecules at Low Energies. *J. Chem. Phys.* **1966**, *45*, 1228−1245.

(24) Simons, J. Propensity Rules for Vibration-Induced Electron Detachment of Anions. *J. Am. Chem. Soc.* **1981**, *103*, 3971−3976.

(25) Liu, H. T.; Ning, C. G.; Huang, D. L.; Wang, L. S. Vibrational Spectroscopy of the Dehydrogenated Uracil Radical by Autodetachment of Dipole-Bound Excited States of Cold Anions. *Angew. Chem., Int. Ed.* **2014**, *53*, 2464−2468.

(26) Zhu, G. Z.; Liu, Y.; Wang, L. S. Observation of Excited Quadrupole-Bound States in Cold Anions. *Phys. Rev. Lett.* **2017**, *119*, 023002.

(27) Yokoyama, K.; Leach, G. W.; Kim, J. B.; Lineberger, W. C.; Boldyrev, A. I.; Gutowski, M. Autodetachment Spectroscopy and Dynamics of Vibrationally Excited Dipole-Bound States of H_2CCC^-. *J. Chem. Phys.* **1996**, *105*, 10706−10708.

(28) Dunbar, R. C. Infrared Radiative Cooling of Gas-Phase Ions. *Mass Spectrom. Rev.* **1992**, *11*, 309−339.

DOI: 10.1021/acs.jpclett.9b01743
J. Phys. Chem. Lett. 2019, 10, 4339−4344

(29) Martin, S.; Bernard, J.; Brédy, R.; Concina, B.; Joblin, C.; Ji, M.; Ortega, C.; Chen, L. Fast Radiative Cooling of Anthracene Observed in a Compact Electrostatic Storage Ring. *Phys. Rev. Lett.* **2013**, *110*, 063003.
(30) Ito, G.; Furukawa, T.; Tanuma, H.; Matsumoto, J.; Shiromaru, H.; Majima, T.; Goto, M.; Azuma, T.; Hansen, K. Cooling Dynamics of Photoexcited C_6^- and C_6H^-. *Phys. Rev. Lett.* **2014**, *112*, 183001.
(31) Henley, A.; Fielding, H. H. Anion Photoelectron Spectroscopy of Protein Chromophores. *Int. Rev. Phys. Chem.* **2019**, *38*, 1−34.
(32) Liu, H. T.; Huang, D. L.; Liu, Y.; Cheung, L. F.; Dau, P. D.; Ning, C. G.; Wang, L. S. Vibrational State-Selective Resonant Two-Photon Photoelectron Spectroscopy of AuS^- via a Spin-Forbidden Excited State. *J. Phys. Chem. Lett.* **2015**, *6*, 637−642.
(33) Becke, A. D. Density-functional thermochemistry. III. The role of exact exchange. *J. Chem. Phys.* **1993**, *98*, 5648−5652.
(34) Tao, J.; Perdew, J. P.; Staroverov, V. N.; Scuseria, G. E. Climbing the Density Functional Ladder: Nonempirical Meta−Generalized Gradient Approximation Designed for Molecules and Solids. *Phys. Rev. Lett.* **2003**, *91*, 146401.
(35) Penfold, T. J.; Gindensperger, E.; Daniel, C.; Marian, C. M. Spin-Vibronic Mechanism for Intersystem Crossing. *Chem. Rev.* **2018**, *118*, 6975−7025.
(36) Schalk, O.; Schuurman, M. S.; Wu, G.; Lang, P.; Mucke, M.; Feifel, R.; Stolow, A. Internal Conversion versus Intersystem Crossing: What Drives the Gas Phase Dynamics of Cyclic *α,β*-Enones? *J. Phys. Chem. A* **2014**, *118*, 2279−2287.
(37) Czekner, J.; Cheung, L. F.; Kocheril, G. S.; Wang, L. S. Probing the Coupling of a Dipole-Bound Electron with a Molecular Core. *Chem. Sci.* **2019**, *10*, 1386−1391.
(38) Reid, K. L. Picosecond Time-Resolved Photoelectron Spectroscopy as a Means of Gaining Insight into Mechanisms of Intramolecular Vibrational Energy Redistribution in Excited States. *Int. Rev. Phys. Chem.* **2008**, *27*, 607−628.

DOI: 10.1021/acs.jpclett.9b01743
J. Phys. Chem. Lett. 2019, 10, 4339−4344